JOURNAL OF GEOPHYSICAL RESEARCH: OCEANS, VOL. 119, 1–12, doi:10.1002/2013JC009450, 2014

A curious local surface salinity maximum in the northwestern tropical Atlantic

Semyon A. Grodsky,[1] James A. Carton,[1] and Frank O. Bryan[2]

Received 18 September 2013; revised 12 December 2013; accepted 28 December 2013.

[1] Sea surface salinity (SSS) measurements from the Aquarius/SAC-D satellite reveal the seasonal development of a local salinity maximum in the northwestern tropical Atlantic in boreal winter to early spring. This seasonal tropical SSS maximum, which is confirmed by comparison to in situ observations, is centered at 8°N, and is up to 0.5 psu saltier than the surrounding water despite its location in the latitude band of the highly precipitating Intertropical Convergence Zone. Its existence seems to be the result of the differing phases in the seasonal variations of Amazon discharge and ocean currents. In late boreal fall, winter, when the discharge is at its minimum, but the North Brazil Current (NBC) and its retroflection are still present, a mixture of high-salinity water of equatorial and South Atlantic origin is transported along the shelf break by the NBC retroflecting into the western part of the North Equatorial Countercurrent (NECC). This salt transport produces the salty signature of the western part of the NECC, which is seen as a localized salinity maximum on satellite imagery, in contrast to the fresh signature present in summer-early fall. The seasonal slowing/reversal of the NECC in boreal spring stops this eastward salt transport, thus leading to the disappearance of this northwestern tropical SSS maximum.

Citation: Grodsky, S. A., J. A. Carton, and F. O. Bryan (2014), A curious local surface salinity maximum in the northwestern tropical Atlantic, *J. Geophys. Res. Oceans*, *119*, doi:10.1002/2013JC009450.

1. Introduction

[2] A striking feature of the Atlantic Ocean is the appearance of pools of high-salinity (>37 psu) surface water in the subtropics of both hemispheres due to high rates of evaporation and negligible rainfall, which are separated by lower-salinity surface water in the rainy tropics [e.g., *Schmitt*, 2008]. The introduction of satellite remote sensing has greatly expanded our ability to monitor the geographical and temporal variability of these sea surface salinity (SSS) features and to detect their variations [*Lagerloef et al*., 2012]. Here we use these new remotely sensed observations to describe the seasonal appearance of a poorly known secondary surface salinity maximum (>36.1 psu) that lies within the high-precipitation tropical zone in the northwestern tropical Atlantic.

[3] The seasonal storage of salt within the mixed layer in this region of the Atlantic is controlled by several competing processes, all of which vary seasonally [*Foltz et al*., 2004]. Among these two major sources of freshwater have to be taken into account: high precipitation under the Intertropical Convergence Zone (ITCZ), and the discharge of major rivers along the northwestern coast of South America [e.g., *Mignot et al*., 2007]. Between the equator and 12°N–15°N mixed layer salinity, and thus SSS is diluted by freshwater input from the seasonally migrating atmospheric ITCZ, which reaches its northernmost position in late boreal summer/fall [e.g., *Xie and Carton*, 2004]. This fresh mixed layer is advected both zonally (by the developing seasonal currents) and meridionally (through Ekman transport by the seasonal trade winds). West of 40°W mixed layer salinity is significantly freshened by the spread of near-surface water from the Amazon, whose discharge peaks in mid-May and decreases to its seasonal minimum in mid-November, reflecting the seasonal march of the ITCZ and water storage processes over the catchment area [*Dai and Trenberth*, 2002]. By early boreal fall, the spread of the Amazon waters forms a 10^6 km^2 fresh pool west of 40°W [*Dessier and Donguy*, 1994], producing near-surface barrier layers capable of affecting local air-sea interactions even under hurricane-force winds [e.g., *Grodsky et al*., 2012]. Barrier layers of up to 20 m thickness have been found equatorward of roughly 10°N except in boreal winter [*Mignot et al*., 2007].

[4] In addition to surface freshwater flux, horizontal advection by seasonal currents also plays an important role in the mixed layer salt balance [e.g., *Foltz et al*., 2004, *Foltz and McPhaden*, 2008; *Grodsky et al*., 2014]. Key features of the seasonal currents [e.g., *Richardson and Reverdin*, 1987] include the westward flowing near-equatorial northern branch of the South Equatorial Current whose

[1]Department of Atmospheric and Oceanic Science, University of Maryland, College Park, Maryland, USA.
[2]National Center for Atmospheric Research, Boulder, Colorado, USA.

Corresponding author: S. A. Grodsky, Department of Atmospheric and Oceanic Science, University of Maryland, College Park, MD 20742, USA. (senya@atmos.umd.edu)

2169-9275/14/10.1002/2013JC009450

J_ID: JGRC Customer A_ID: JGRC20542 Cadmus Art: JGRC20542 Ed. Ref. No.: 2013JC009450RR Date: 7-January-14 Stage: Page: 2

transport peaks in boreal summer, and feeds into the coastal North Brazil Current (NBC). The NBC transports this water, diluted by discharge from the Amazon River, northwestward along the eastern boundary of South America in boreal winter and spring. In summer, however, the shifting trade winds allow the NBC to retroflect and be carried eastward in the developing North Equatorial Countercurrent (NECC) at latitudes between 5°N and 10°N [e.g., *Carton and Katz*, 1990]. Indeed, from August to October typically 70% of the Amazon plume water is deflected eastward in the NECC along the NBC retroflection [*Lentz*, 1995], thus producing the fresh signature of the western part of the NECC present in summer-early fall. The seasonal appearance of the fresh NECC and accompanying ITCZ rainfall dramatically reduce mixed layer salinities in this band of latitudes [*Muller-Karger et al*., 1988], causing a fresh barrier layer to develop within the mixed layer [e.g., *Liu et al*., 2009]. The western part of the NECC reaches its maximum eastward flow by boreal fall, then slows so that in late boreal winter the direction of the surface current is westward. As we shall see later, the seasonal changes of salinity of water carried by the NBC into the NECC ultimately leads to the seasonal appearance of a local surface salinity maximum pool in the western basin.

[5] Until recently most of the information about these changes in salinity came from a series of in situ observing programs such as the volunteer observing ship thermosalinograph (TSG) program [e.g., *Dessier and Donguy*, 1994], historical hydrography available in the World Ocean Atlas series such as WOA09 [*Boyer et al*., 2012], as well as the recently deployed Argo profiling floats [*Roemmich et al*., 2009]. In the past several years, this suite of in situ salinity measurements has been complemented by observations from two remote sensing instruments: the Soil Moisture and Ocean Salinity satellite in late-2009 and Aquarius/SAC-D in spring 2011. Both instruments observe upwelling radiation in the microwave L-band (1.4 GHz) and deduce salinity from the emissivity dependence on surface conductivity. In this study, we examine Aquarius/SAC-D observations, which have a spatial resolution of approximately 100 km [*Lagerloef et al*., 2012]. The results are diagnosed by comparison to salinity from more traditional observing systems and an eddy resolving ocean numerical simulation.

2. Data and Methods

[6] The main SSS data set used in this study is the daily level 3 version 2.3 Aquarius SSS beginning 25 August 2011 obtained from the NASA Jet Propulsion Laboratory Physical Oceanography Distributed Active Archive Center on a $1^\circ \times 1^\circ$ grid [*Lagerloef et al*., 2012], which spans only two full years so far. To emphasize features present during both years, the Aquarius SSS climatology is evaluated using the Fourier series truncated after the annual and semiannual harmonics. In the tropics where the seasonal variations dominate, it is reasonable to examine such a SSS climatology based on only 2 years of observations because of the dominance of the annual cycle [e.g., *Xie and Carton*, 2004]. We will illustrate the similarity of SSS between 2012 and 2013 later.

[7] The Aquarius SSS data are used along with the salinity observations from four buoys located between 4°N and 15°N along the 38°W meridian [*Foltz et al*., 2004]. These buoys, which are part of the Prediction and Research Moored Array in the Atlantic (PIRATA) array [*Bourlès et al*., 2008], have been maintained continuously since 1997. Salinity is typically available at four depths between 1 and 120 m. We also use the monthly WOA09 SSS climatology based on historical hydrographic observations [*Boyer et al*., 2012]; ship of opportunity TSG data collected along major merchant ship lanes [*Dessier and Donguy*, 1994]; and the uppermost measurement from Argo profiling floats (typically at 5–10 m depth) [*Roemmich et al*., 2009].

[8] In the latitude band of the highly precipitating ITCZ, much of the temporal variability of net surface freshwater flux is due to the temporal variability of precipitation [*Yoo and Carton*, 1990]. We track variations in precipitation using a combination of the Microwave Imager and the Precipitation Radar that form part of the Tropical Rainfall Measuring Mission (TRMM) satellite sensor suite (trmm.gsfc.nasa.gov). We track monthly continental discharge from ~~the~~ tropical South America by combining the Amazon discharge at Obidos with discharges from the two major Amazon tributaries downstream of Obidos (Tapajos and Xingu), and adding the Tocantins River discharge. These discharge data are obtained from the HYBAM observatory (www.ore-hybam.org) and the Brazilian water agency (www.ons.org.br/operacao/vazoes_naturais.aspx). We estimate horizontal salt transport using climatological near-surface currents based on observations of 15 m depth currents from the Global Drifter Program [*Lumpkin and Garrafo*, 2005].

[9] The observations cannot resolve small-scale processes such as eddy advection. To quantify these unresolved processes, we compare the salt budget to that derived from an eddy resolving simulation using Parallel Ocean Program (POP2, version 2) numerics. The model configuration is described by *Maltrud et al*. [2010]. The grid has the nominal longitudinal resolution of 0.1° with a global tripole grid, and 42 vertical levels with approximately 10–15 m resolution in the upper 100 m. Mixed layer physics is included using the K-Profile Parameterization of *Large et al*. [1994]. Atmospheric forcing is based on the normal-year forcing of the Coordinated Ocean Reference Experiment (CORE) [*Large and Yeager*, 2004]. Monthly river runoff from 46 major rivers is added to the surface fresh water flux at the locations of the actual outflow as an implied negative salt flux. The model computes all terms of the salt budget as an inline calculation on the original model grid as 5 day averages. Here we examine the final 3 years of a 68 year simulation starting from annual mean temperature and salinity from the World Ocean Circulation Experiment (WOCE) Global Hydrographic Climatology of *Gouretski and Koltermann* [2004].

[10] Using the model ~~data~~, we evaluate the terms in the salt budget within the mixed layer (depth $H(x,y,t)$). Vertically averaging the salt transport equation over depth $H(x, y, t)$ gives:

$$\underbrace{<\frac{\partial S}{\partial t}>}_{TEND} = \underbrace{-<u\frac{\partial S}{\partial x}>}_{ZADV\_T} \underbrace{-<v\frac{\partial S}{\partial y}>}_{MADV\_T} \underbrace{-<w\frac{\partial S}{\partial z}>}_{VADV\_T} + \underbrace{\frac{(E-P)S}{H}}_{SSF} + \underbrace{\frac{Q_{DIF}(z=H)}{H}}_{VDIF} + <HDIF> \quad (1)$$

ID: padmavathym Time: 13:47 I Path: //xinchnasjn/01journals/Wiley/3B2/JGRC/Vol00000/140002/APPFile/JW-JGRC140002

J_ID: JGRC Customer A_ID: JGRC20542 Cadmus Art: JGRC20542 Ed. Ref. No.: 2013JC009450RR Date: 7-January-14 Stage: Page: 3

where $< >$ denotes the vertical average over the mixed layer. The terms in (1) are: salt tendency (TEND); total zonal (ZADV_T), meridional (MADV_T), and vertical (VADV_T) salt advection components; surface salt flux (SSF) and vertical diffusion (VDIF) across $z=H(x,y,t)$ scaled by the mixed layer depth; and horizontal diffusion (HDIF). Each total salt advection component is further decomposed into two parts, such as zonal advection by monthly mean currents $\mathrm{ZADV} = <\overline{u}\partial\overline{S}/\partial x>$, and zonal eddy advection by intramonth variations, $\mathrm{ZEDDY} = <\overline{u'\partial S'/\partial x}>$. The overbar represents a running quasimonthly average (actually a 35 day average, which is the closest estimate of centered monthly mean at 5 day decimation). Here and after ZADV, MADV, and VADV refer to advection components by monthly mean currents, while ZEDDY, MEDDY, and VEDDY stand for eddy salt advection components by intramonth variations. The sum of the two horizontal components of salt advection is referred to as horizontal salt advection (HADV = ZADV + MADV; HEDDY = ZEDDY + MEDDY). The separation between mean and eddy time scales at 1 month is somewhat arbitrary because the time scale of separation between the seasonal forcing and mesoscale variability is not really sufficient to define a clear-cut division. HDIF varies on small (a few grid points) spatial scales in the open ocean and its contribution to the spatial mean is normally negligible.

3. Results

3.1. Observations

[11] We begin by examining the seasonal cycles of the Amazon discharge and the strength of the NBC retroflection (Figure 1). Zonal velocity averaged over the western part of NECC provides a proxy for the strength of the retroflection [*Garzoli et al*., 2004; *Lumpkin and Garzoli*, 2005] and shows that the retroflection is still in place in late boreal fall winter when continental, primarily Amazon discharge drops to its seasonal minimum. This difference in annual phases leads to important changes in the salinity of water carried northwestward by the NBC into the retroflection. During boreal summer to early fall, when Amazon discharge is rather strong, freshwater is entrained into the NBC and is transported to the east along the retroflection. This produces a fresh signature along the path of the NECC. This circulation is nicely visualized by ocean color [e.g., *Muller-Karger et al*., 1988], which shows how turbid river water extends east into the interior Atlantic. As the year progresses and Amazon discharge weakens, the same circulation provides a very different contribution to salt transport.

[12] Amazon discharge reaches low levels in October even though the fresh plume is still distinguishable from the higher SSS background (Figure 2a). During that month freshwater carried eastward by the retroflection is further diluted by local rainfall as water parcels are advected eastward, thus reinforcing the fresh pattern in the western part of the NECC. By December, the Amazon plume has shrunk toward the coast (compare Figures 2b and 2a) reflecting the seasonal decrease in the discharge (Figure 1a) and increase in mixing due to strengthening winds [*Grodsky et al*., 2012].

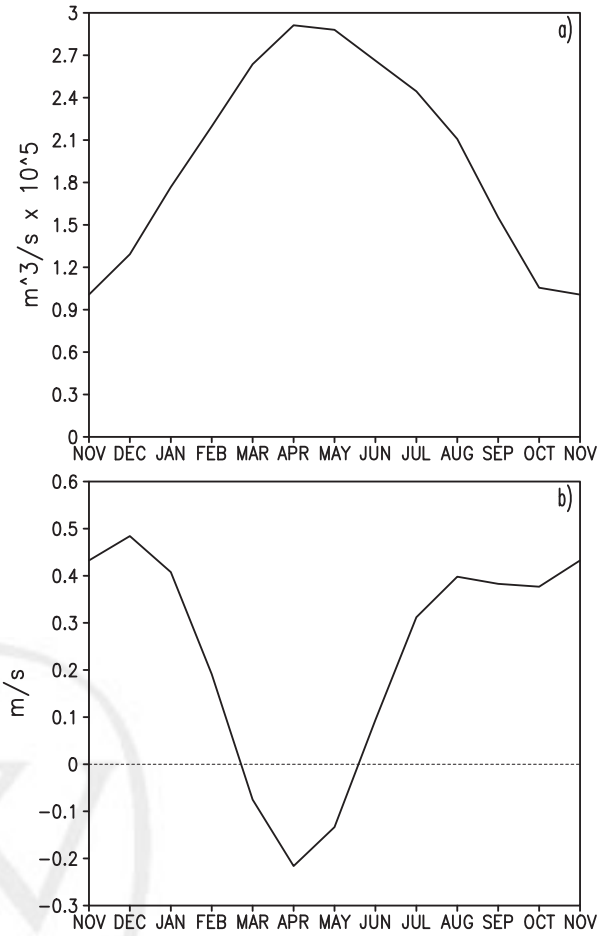

Figure 1. Climatological monthly (a) discharge from the tropical South American rivers (combined discharge of the Amazon at Obidos, the two major Amazon tributaries: downstream of Obidos (Tapajos and Xingu), and the Tocantins River); (b) zonal surface drifter velocity averaged in the western part of region containing the North Equatorial Countercurrent (45°W–35°W, 5°N–8°N) (see Figure 2b for the box location).

[13] The development of a local SSS maximum, which is centered at around 8°N and extends beyond 30°W, begins in December (Figure 2b). In this month, advection of salty NBC water eastward by the NECC, which is now only weakly diluted by the Amazon, acts to increase the salinity of the western part of the NECC, opposing the freshening effects of local rainfall. In the following couple of months, this eastward salt transport dominates the diluting effects of local rainfall causing the SSS maximum to grow in spatial extent and magnitude (Figures 2c and 2d). This growth is also related to the southward shift of the ITCZ, reducing local rainfall.

[14] By early northern spring (Figure 2e), the retroflection starts weakening, thus decreasing the eastward salt transport into the SSS maximum region. The SSS maximum is still distinguishable, but it is shifted northward by local wind-driven currents (so that the center has shifted to around 10°N in March). In the following months, northward advection of this SSS maximum region causes it to merge with the main subtropical salty pool by May (Figure

ID: padmavathym Time: 13:47 I Path: //xinchnasjn/01journals/Wiley/3B2/JGRC/Vol00000/140002/APPFile/JW-JGRC140002

J_ID: JGRC Customer A_ID: JGRC20542 Cadmus Art: JGRC20542 Ed. Ref. No.: 2013JC009450RR Date: 7-January-14 Stage: Page: 4

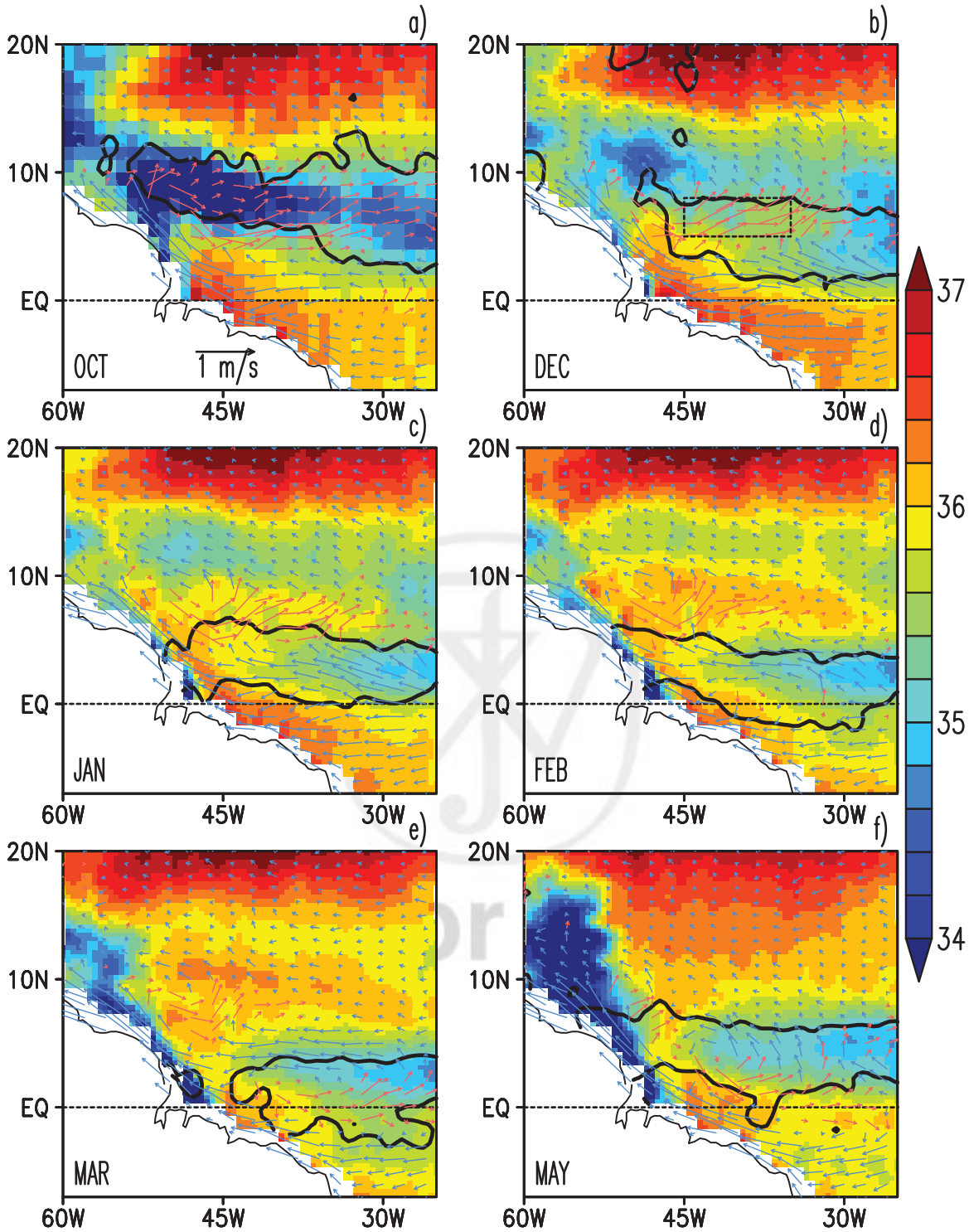

Figure 2. Monthly averaged climatological Aquarius SSS (shading), surface drifter currents (arrows), and TRMM rainfall (6 mm/d contour). (b) The western NECC region (45°W–35°W, 5°N–8°N) is outlined in red. Climatological SSS is constructed by the annual and semiannual harmonics.

2f). By early summer, the newly invigorated Amazon plume has developed and its freshwater begins to be entrained into the NECC.

[15] Another distinctive feature of the tropical local SSS maximum is related to the presence of the two bounding fresh bands of SSS to the north and south. In January to February SSS is generally below 36 psu, reaching a zonally averaged minimum of 35.5 psu under the ITCZ rain band centered at around 4°N (Figure 3). But, further north there is another SSS minimum between 10°N and 15°N, well north of the ITCZ during these months (see Figure 4a for the ITCZ latitude). These two fresh bands bound the local

ID: padmavathym Time: 13:47 I Path: //xinchnasjn/01journals/Wiley/3B2/JGRC/Vol00000/140002/APPFile/JW-JGRC140002

J_ID: JGRC Customer A_ID: JGRC20542 Cadmus Art: JGRC20542 Ed. Ref. No.: 2013JC009450RR Date: 7-January-14 Stage: Page: 5

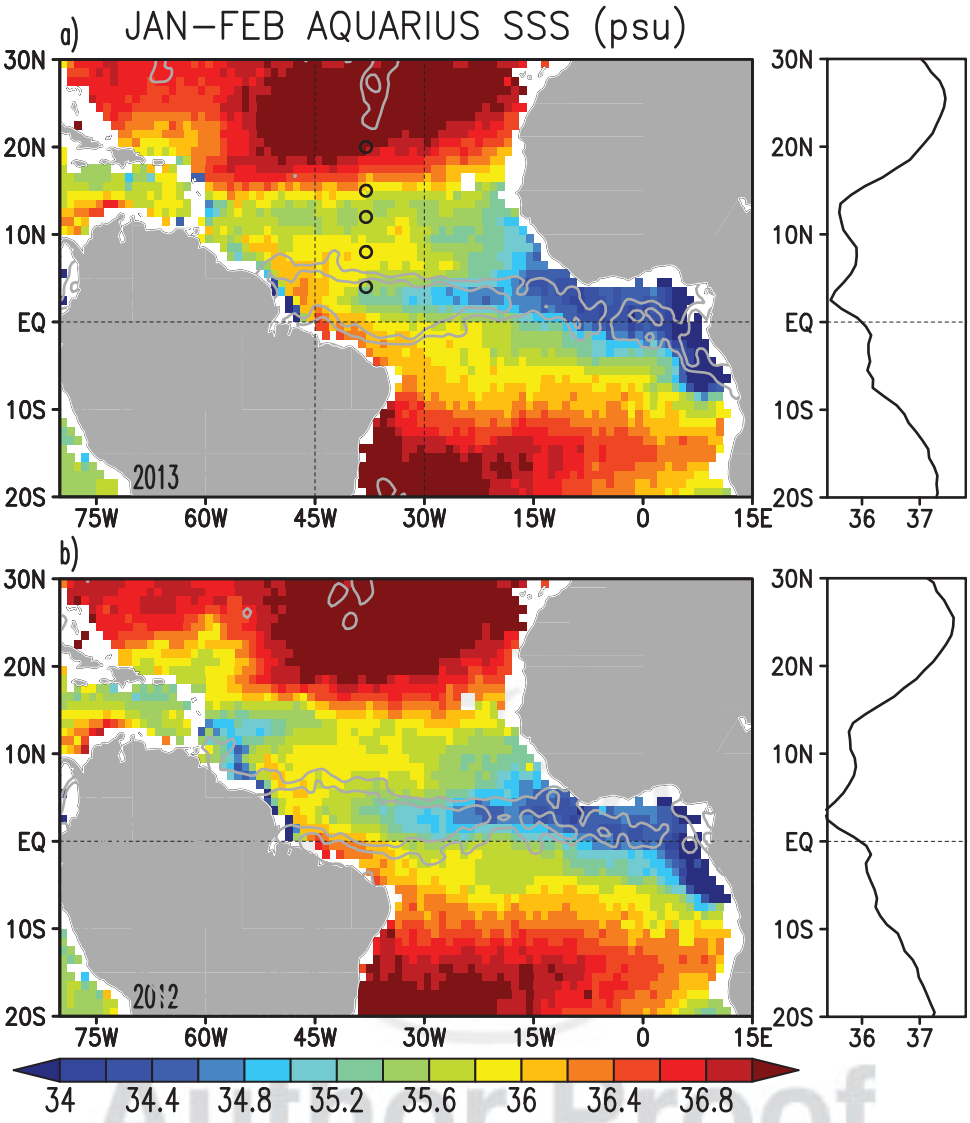

Figure 3. January to February Aquarius SSS in (a) 2013 and (b) 2012 (shaded). Also shown are: TRMM rainfall (3 and 6 mm/d, gray contours) and the 38°W PIRATA mooring locations (open circles). (right) SSS zonally averaged 45°W–30°W.

SSS maximum that is centered at around 8°N. All these SSS features are present during January to February of both 2012 and 2013 suggesting that they belong to the seasonal cycle of SSS in the northwestern tropical Atlantic. The similarity of SSS patterns observed during the 2 years of Aquarius observations (Figure 3) illustrates the dominance of the seasonal cycle in the tropical Atlantic [see also *Xie and Carton*, 2004] and justifies (in part) our use of a SSS climatology (Figure 2), which is derived from only 2 years of data. However, we also note that interannual changes in the magnitude and position of the SSS maximum are present, although their origins are yet to be explored (compare Figures 3a and 3b).

[16] The fortuitous location of the PIRATA moorings along 38°W (see Figure 3a) allows us to look at the seasonal appearance and vertical structure of this salinity maximum based on a 15 year climatology. At this longitude, the ITCZ and its associated rainfall maximum is pushed northward to a seasonal maximum latitude of 8°N in August before descending to around 2°N during boreal winter to spring (January to April) as shown in Figure 4a. SSS at 4°N is at its seasonal minimum in May to June (Figure 4b) following the northward shift of the ITCZ past this latitude in boreal spring. The seasonal maximum at this location, which is only 0.25 psu higher than this minimum, occurs in boreal fall and early winter when horizontal advection controls surface salinity [*Foltz et al.*, 2004].

[17] Like the spring minimum at 4°N, the minimum SSS at 8°N of 34.5 psu occurs in fall in response to the local appearance of the ITCZ and the contribution of freshwater transport by the NECC. SSS increases by 1.5 psu during the first half of the year when both contributions weaken. As the year progresses, this salty water becomes overlain by newly rainfall-diluted surface water. From the middle of boreal spring through the second half of the year, the water from the surface salinity maximum occurs also at

ID: padmavathym Time: 13:47 I Path: //xinchnasjn/01journals/Wiley/3B2/JGRC/Vol00000/140002/APPFile/JW-JGRC140002

J_ID: JGRC Customer A_ID: JGRC20542 Cadmus Art: JGRC20542 Ed. Ref. No.: 2013JC009450RR Date: 7-January-14 Stage: Page: 6

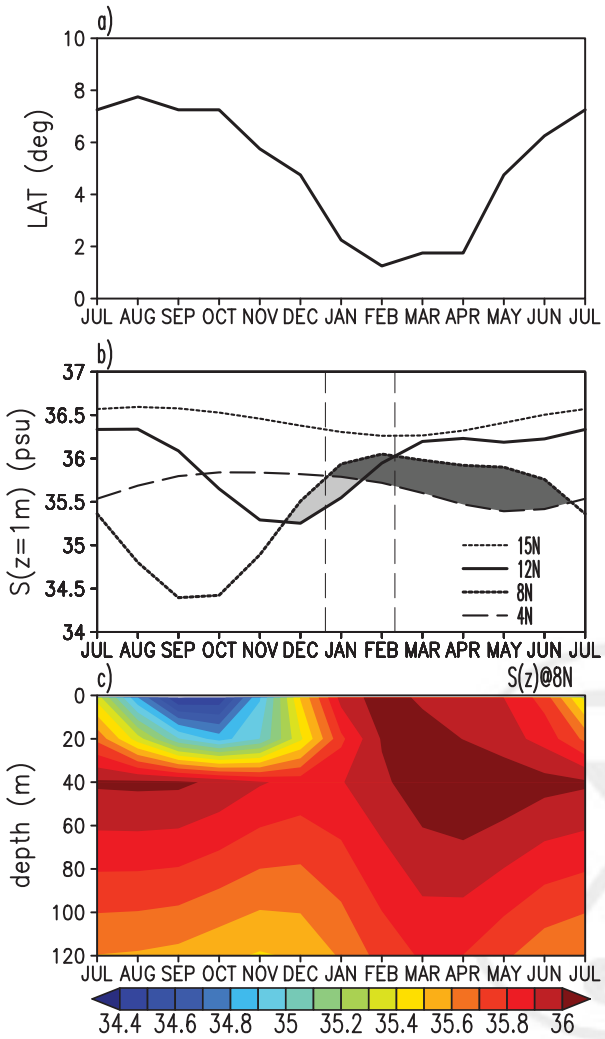

Figure 4. Seasonal cycle at 38°W of (a) latitude of maximum rainfall, (b) 1 m depth salinity (S) at PIRATA moorings, (c) salinity with depth at the 8°N PIRATA mooring. In Figure 4b, $S(8°N) > S(12°N)$ and $S(8°N) > S(4°N)$ are shaded in light and dark gray, respectively. PIRATA salinity is available at 1, 20, 40, and 120 m levels. Vertical profiles below 40 m are not resolved well because no data are available between 40 and 120 m levels.

subsurface levels, extending down to at least 40 m depth, where it can become involved in equatorward transport within the shallow tropical cell (Figure 4c).

[18] The seasonal cycle of SSS at 12°N (Figure 4b) is different from that of either 4°N or 8°N in that it reaches a minimum of 35.25 psu in November to December, 2 months after the minimum at 8°N. In the western tropical Atlantic, the ITCZ core does not reach 12°N (see Figure 4a). Hence, the ITCZ rainfall stops earlier at 12°N than at 8°N. If rainfall were the only cause of freshening at 8°N and 12°N, the minimum SSS would occur earlier at 12°N. But, the SSS minimum at 12°N occurs 2 months behind the timing of the minimum at 8°N. This is *well after* the maximum in local rainfall and occurs at a time when the ITCZ is shifting southward. This 2 month time lag relative to 8°N, as we will see later, is caused by the time delay associated with meridional salt advection. High (>36.25 psu) salinities gradually return at 12°N by March, similarly lagging SSS at 8°N. The combined effects of the weak seasonal cycle at 4°N and the delay of the seasonal cycle at 12°N relative to 8°N mean that for the 2 month period, January to February, SSS is locally maximum at 8°N.

[19] Finally, we examine the temporal evolution of SSS for the longitude band 45°W–30°W in the western tropical Atlantic (see Figure 3a) from fall of 2011 through spring of 2013 (Figure 5). The water is freshest at around 8°N in boreal fall, a season when the ITCZ is close to its seasonal maximum latitude. At this time, the mixed layer at 8°N is shallow, and there is additional dilution by eastward Amazon water transport [*Foltz et al.*, 2004; *Foltz and McPhaden*, 2008]. Even though the ITCZ starts declining southward in November, this residual band of fresh SSS at 8°N is gradually advected northward at a rate of about 4 cm/s, freshening the surface layers to the north, finally reaching 15°N by boreal spring (Figures 4b and 5). It is this slow advective time scale that explains the delayed seasonal cycle at 12°N. South of 8°N SSS also drops to its seasonal minimum in boreal spring, but in this case in response to an increase in local rainfall. The result of these two different processes is the appearance of the 0.5 psu local salinity maximum in boreal winter to early spring in between the two fresh bands. While the moored time series make clear that the processes controlling salinity at these locations are highly seasonal, comparison of the 2 years of data suggests that the salinity maximum was more pronounced (by a fraction of a psu) in 2013 than in 2012 (Figures 3 and 5).

3.2. Model

[20] Similar to what is suggested by observed SSS shown in Figure 2, the simulation shows salty surface water from the southwestern equatorial Atlantic is being transported by the NBC northwestward along the coast (Figure 6). This salty water isolates the water diluted by weak Amazon discharge near the coast from the water in the interior. When the NBC retroflects eastward, it carries this salty water into the western part of NECC (which is centered at 6°N in this model snapshot). The salty water is then advected eastward by the meandering NECC and is still distinguishable from the fresher SSS to the north and south until it reaches approximately 30°W (Figure 6). Again consistent with the observations (Figure 2), the fresh band to the south is collocated with the ITCZ and appears to be the result of local rainfall and salt advection [e.g., *Foltz et al.*, 2004], whilst the freshwater to the north of the NECC is not. We next evaluate the salt budget within the mixed layer contained in the NECC box and the northern "fresh" box (see Figure 6). Our goal is to quantify mechanisms discussed qualitatively above.

[21] In the northern box (Figure 7a), SSS varies annually reaching minimum in late fall (compare to the 12°N PIRATA salinity in Figure 4b). Mixed layer depth is impacted by salinity. It is shallower than 30 m in fall winter when the mixed layer freshens and deepens below 50 m when mixed layer gets saltier. This annual change in the mixed layer salinity (Figure 7b) is balanced by a combination of SSF, meridional advection by monthly mean currents, MADV = $<\bar{v}\partial\overline{S}/\partial y>$, and VDIF (Figure 7b).

ID: padmavathym Time: 13:48 I Path: //xinchnasjn/01journals/Wiley/3B2/JGRC/Vol00000/140002/APPFile/JW-JGRC140002

J_ID: JGRC Customer A_ID: JGRC20542 Cadmus Art: JGRC20542 Ed. Ref. No.: 2013JC009450RR Date: 7-January-14 Stage: Page: 7

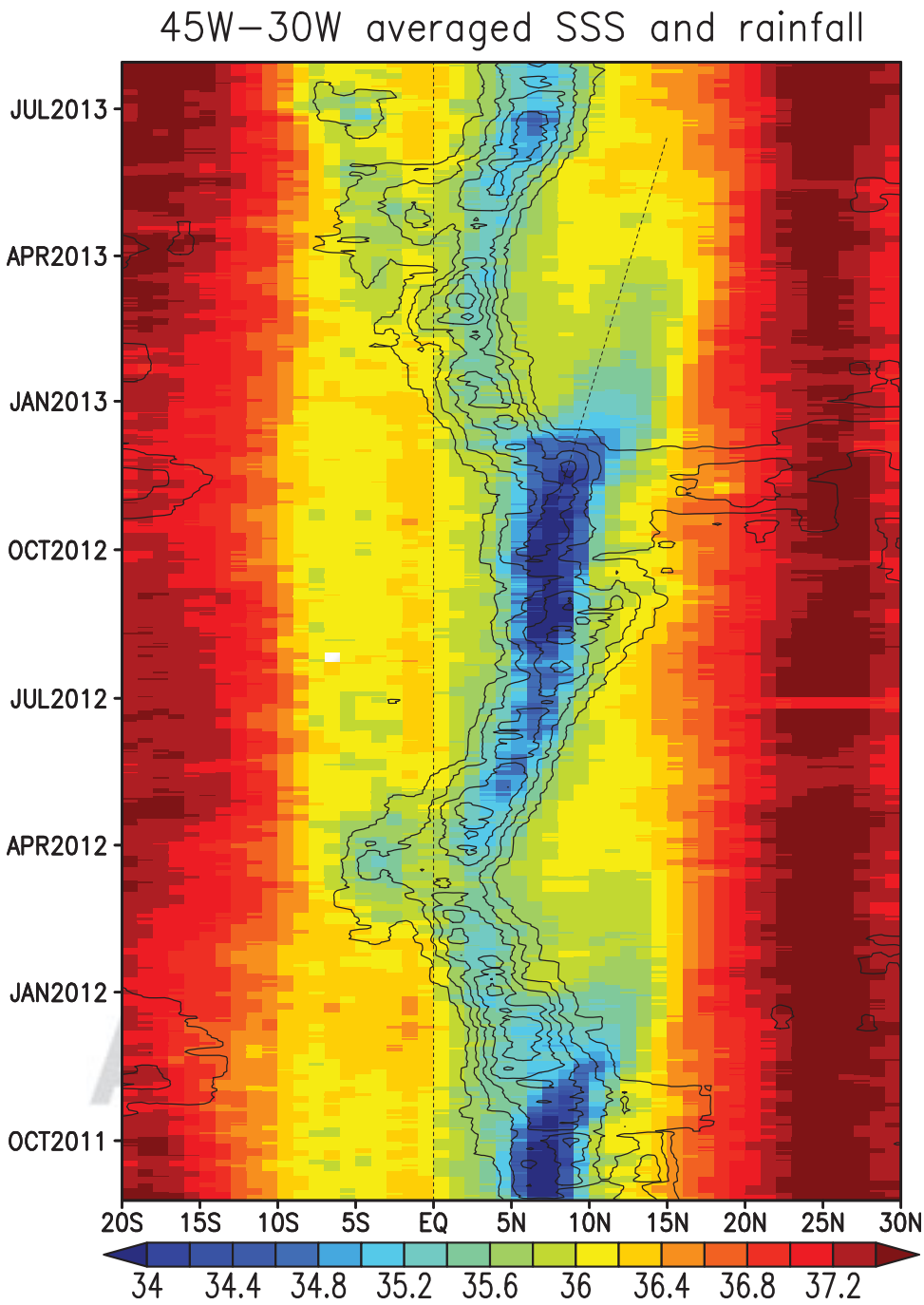

Figure 5. AQUARIUS SSS (psu, shaded) and TRMM rainfall >3 mm/d (CI = 3 mm/d) averaged 45°W–30°W. Slope line corresponds to 4 cm/s northward propagation.

Indeed, these three terms explain more than 90% of the variance of TEND in this northern box. The remaining variance is explained by the horizontal eddy flux by intramonth variations, HEDDY = $<\overline{u'}\partial S'\partial x+\overline{v'}\partial S'\partial y>$ (Figure 7c).

[22] TEND in the northern box can be separated into one period during which it is positive from late boreal fall through middle of summer and a second when it is negative for the remainder of the year (Figure 7b). Different processes dominate during these two periods (Figure 7c). The seasonal changes in TEND vary mostly in phase with SSF and MADV both of which are linked to the seasonal changes in the ITCZ latitude and its impact on wind speed and precipitation. The SSS rise during the first period (when the ITCZ shifts south) is mostly driven by net evaporation (SSF > 0) overcoming freshening by meridional advection. In contrast, the SSS decline during the second period is mainly the result of meridional advection by monthly mean currents of fresher water from the south (MADV < 0). Freshening SSS sharpens the halocline below the base of the mixed layer (Figure 7a), in turn leading to a negative feedback on the mixed layer salinity via positive

ID: padmavathym Time: 13:48 I Path: //xinchnasjn/01journals/Wiley/3B2/JGRC/Vol00000/140002/APPFile/JW-JGRC140002

J_ID: JGRC Customer A_ID: JGRC20542 Cadmus Art: JGRC20542 Ed. Ref. No.: 2013JC009450RR Date: 7-January-14 Stage: Page: 8

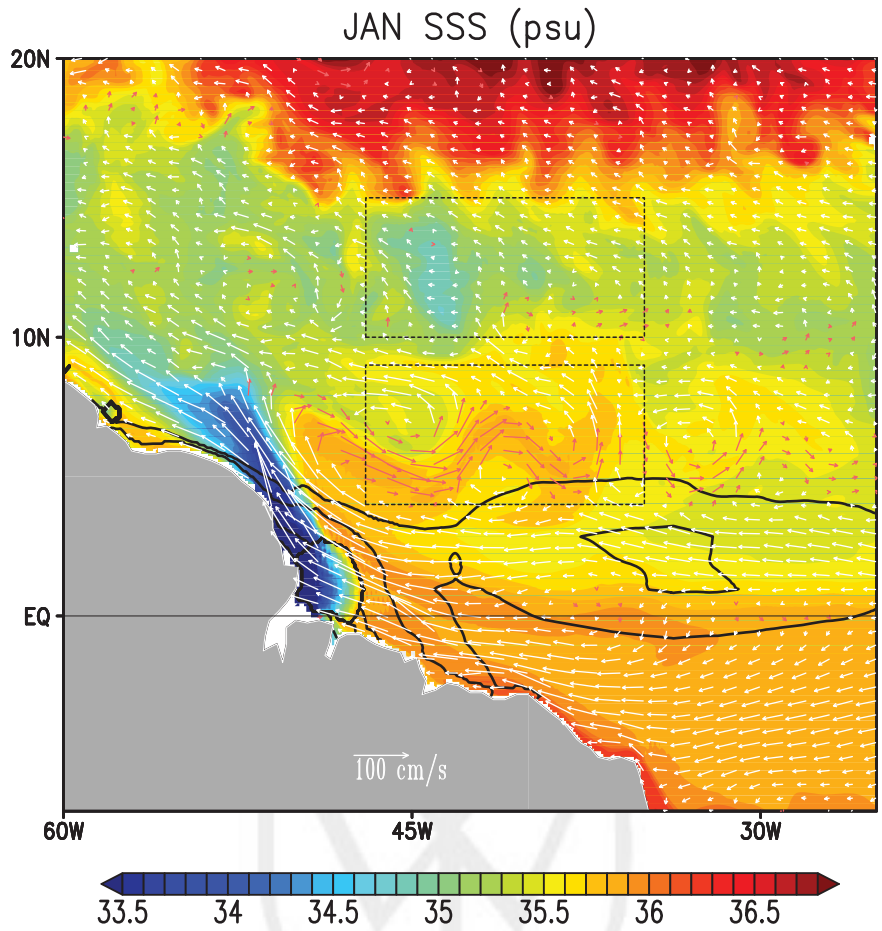

Figure 6. January simulated SSS (model year 67, psu, shaded), surface currents (arrows, westward white, eastward red), and net surface freshwater flux (P-E, 2.5 mm/d, 5 mm/d contours). Two boxes: a northern box (47°W–35°W, 10°N–15°N) and an NECC box (47°W–35°W, 4°N–9°N) are selected for salt budget analysis in Figure 7.

vertical diffusive salt flux, VDIF > 0 (Figure 7c). Horizontal eddy flux (HEDDY) provides seasonally varying freshening to the northern box. Vertical eddy flux, $<\underline{w'\partial S'/z}>$, in contrast, is positive, but its magnitude ~0.1 psu/yr is small. The sum of SSF, MADV, VDIF, and HEDDY (not shown) is almost equal to TEND suggesting that contribution of the other terms to the salt budget of the northern box is negligible.

[23] The seasonal cycle of mixed layer salinity in the NECC box (Figure 8) is also dominated by its annual harmonics. Maximum freshening occurs in September to October in line with the 8°N PIRATA observations (Figure 4b). The periods of positive and negative TEND and horizontal advection by monthly mean currents (HADV) occur in phase and have similar magnitude suggesting that TEND and HADV almost balance each other (Figure 8b). Other terms in the salt budget are not negligible, but their combined effect is less than that of HADV. In particular, VDIF acts to increase the salinity of the mixed layer due to the presence of higher-salinity water below the mixed layer. But, it varies out of phase with SSF, thus leading to partial compensation of the two. As illustrated in Figure 2 for the observations and Figure 6 for the simulation, positive salt transport along the NECC (HADV > 0) acts against the freshening effects of dilution by rain during late fall and winter. The three-dimensional eddy salt flux (EDDY = HEDDY + VEDDY) is variable in time reflecting an eddy-induced sloping and meandering of isopycnal surfaces. This intrinsic ocean variability in the western part of the NECC is complex even in an ocean driven by climatological forcing, but is smaller in size than other terms shown in Figure 8c because of compensation between HEDDY and VEDDY.

[24] Thus, the salt budget partitioning shown in Figure 8b confirms that the seasonal salinity changes in the western part of NECC are dominated by horizontal salt transport by the monthly mean NECC. This salt transport produces a familiar fresh signature of the western part of NECC in boreal summer-early fall. But during late fall and winter, when dilution by Amazon discharge is minimal even though the NECC is still flowing, it produces a salty signature in the western part of the NECC, which is seen as the local SSS maximum apparent in Aquarius SSS. There is clearly some year-to-year variability in the ocean simulations driven by annually repeating forcing, e.g., Figure 8b, that is included in monthly mean advection. Perhaps, the

ID: padmavathym Time: 13:48 I Path: //xinchnasjn/01journals/Wiley/3B2/JGRC/Vol00000/140002/APPFile/JW-JGRC140002

J_ID: JGRC Customer A_ID: JGRC20542 Cadmus Art: JGRC20542 Ed. Ref. No.: 2013JC009450RR Date: 7-January-14 Stage: Page: 9

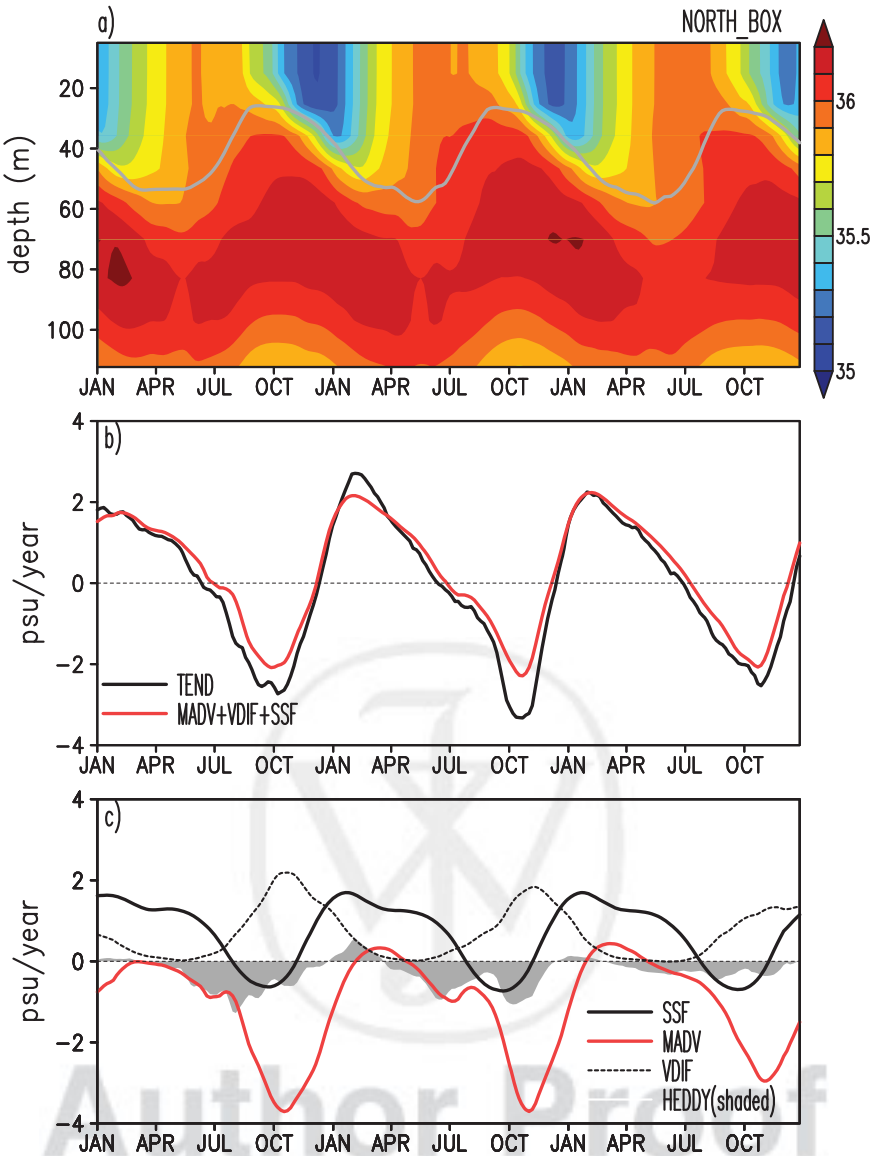

Figure 7. Mixed layer salt budget spatially averaged over the northern box (see Figure 6): (a) box averaged salinity (psu) and mixed layer depth (H); (b) salt tendency (TEND) and the sum of surface salt flux (SSF), meridional advection by monthly currents (MADV), and vertical salt diffusion across the mixed layer base (VDIF); (c) budget terms shown separately including the horizontal eddy salt flux (HEDDY) by intramonth oscillations.

eddy terms in Figures 7 and 8 might be considered as providing lower bounds for the contribution of intrinsic oceanic variability.

4. Summary and Discussions

[25] New satellite remote sensed SSS observations from the Aquarius/SAC-D satellite reveal the seasonal development of a 0.5 psu local SSS seasonal maximum in the northwestern tropical Atlantic during boreal winter to early spring. This maximum is centered on 8°N and is the result of the different seasonal phase of the strength of continental, primarily Amazon discharge and the appearance of the NBC retroflection. In boreal fall, when the discharge is at its minimum, but the NBC retroflection and the eastward NECC are still present, salty surface water of equatorial and Southern Hemisphere origin is retroflected into the western part of the NECC. The seasonal weakening and reversal of the NECC in boreal spring stop this eastward salt transport, thus leading to the disappearance of this local salinity maximum. Depth resolving PIRATA salinity records suggest that water from this surface salinity maximum may interact with water from the subsurface salinity maximum, thus interacting with equatorward transport within the shallow tropical cell.

[26] This tropical SSS maximum in boreal winter is bounded by two bands of fresh SSS to the north at 10°N–15°N and to the south at 4°N. The fresh band to the south is diluted by local rainfalls which intensify by late winter, but a previous study suggests that salt advection is also

ID: padmavathym Time: 13:48 I Path: //xinchnasjn/01journals/Wiley/3B2/JGRC/Vol00000/140002/APPFile/JW-JGRC140002

J_ID: JGRC Customer A_ID: JGRC20542 Cadmus Art: JGRC20542 Ed. Ref. No.: 2013JC009450RR Date: 7-January-14 Stage: Page: 10

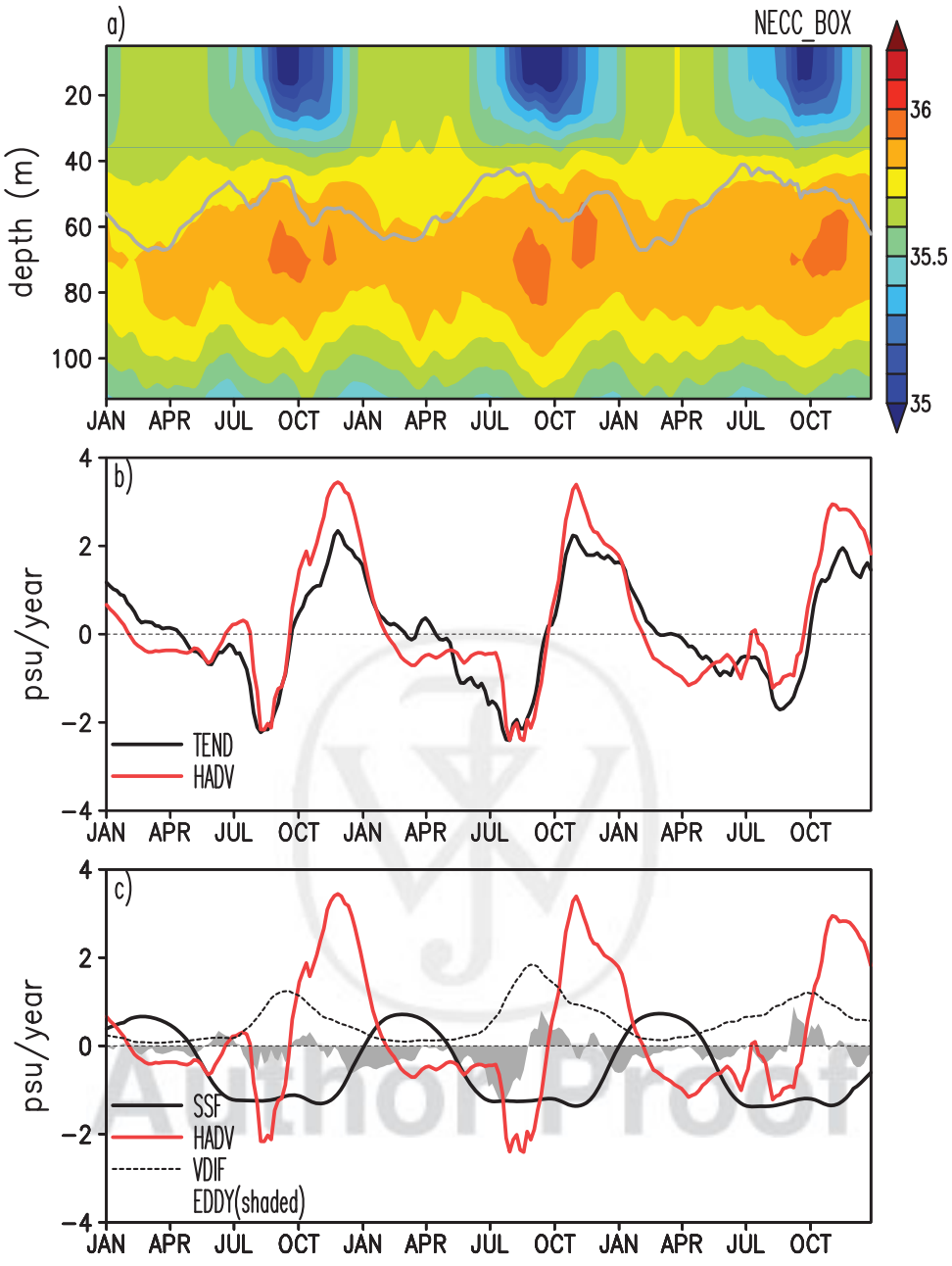

Figure 8. Mixed layer salt budget spatially averaged over the NECC box (see Figure 6): (a) horizontally averaged salinity (psu) and mixed layer depth (H); (b) salt tendency (TEND) and horizontal advection by monthly currents (HADV); (c) budget terms shown separately including the 3-D eddy salt flux (EDDY) by intramonth oscillations. Note that temporal changes of horizontally averaged salinity and H in Figure 8a do not match in this high-gradient region.

important here [*Foltz et al*., 2004]. North of 8°N seasonal rains is dramatically weaker in the western tropical Atlantic. The fresh mixed layer observed in the northern band results from the northward transport of fresher surface water from lower latitudes originated during the previous summer-early fall when it was diluted by rainfall and advected Amazon River discharge. Between the two fresh bands SSS reaches a maximum at 8°N early in the calendar year due to weakening rain and an increase in the eastward exchange of salty water.

[27] There is some evidence of this local salinity maximum in historical observations in the ships of opportunity thermosalinograph climatology of *Dessier and Donguy* [1994] (Figure 9a). But in the hydrography-based World Ocean Atlas of *Boyer et al*. [2012], the local SSS maximum is almost missing (Figure 9b). Our own compilation of the more recent observations from the Argo profiling floats [*Roemmich et al*., 2009] using observations in the 5–10 m depth range as a proxy for SSS does indicate the presence of this local salinity maximum. However, the limitations

ID: padmavathym Time: 13:48 I Path: //xinchnasjn/01journals/Wiley/3B2/JGRC/Vol00000/140002/APPFile/JW-JGRC140002

J_ID: JGRC Customer A_ID: JGRC20542 Cadmus Art: JGRC20542 Ed. Ref. No.: 2013JC009450RR Date: 7-January-14 Stage: Page: 11

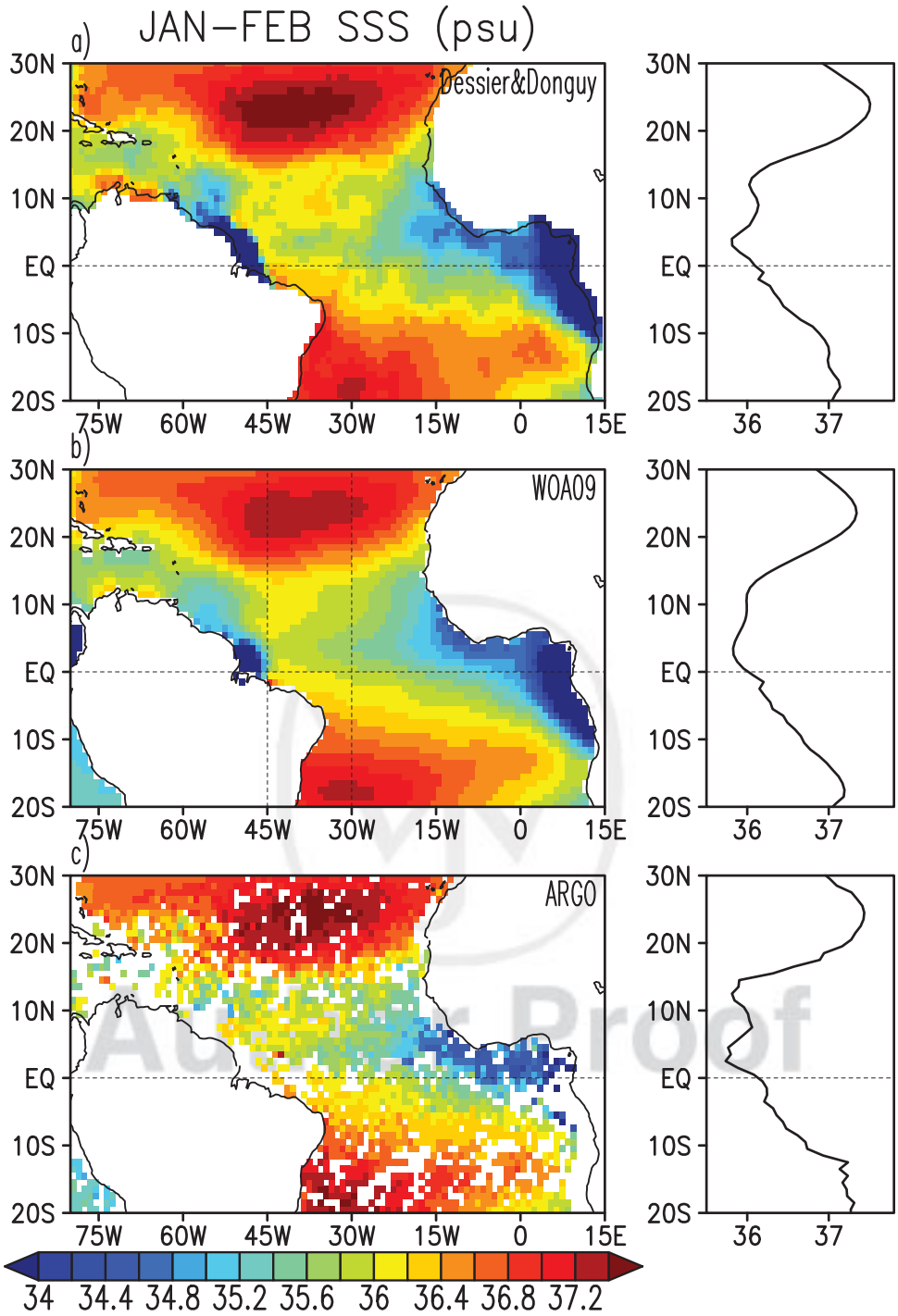

Figure 9. January to February SSS climatology from (a) *Dessier and Donguy* **[**1994**]**, (b) WOA09, and (c) based on Argo float observations. (right) SSS averaged 45°W–30°W.

introduced by Argo operation in the shelf regions and by the fact that Argo sampling begins at 5–10 m depth are indicated by the fact that this analysis misses the Amazon plume altogether (Figure 9c).

[28] **Acknowledgments.** This research was supported by the NASA (NNX12AF68G, NNX09AF34G, and NNX10AO99G). F.**B.** was supported by the National Science Foundation through its sponsorship of the National Center for Atmospheric Research. The continental discharge is provided by the HYBAM observatory and the Brazil Water Agency. We acknowledge the TAO Project Office of NOAA/PMEL for making the PIRATA data freely available.

References

Bourlès, B., et al. (2008), The Pirata program: History, accomplishments, and future directions, *Bull. Am. Meteorol. Soc.*, *89*, 1111–1125.

Boyer, T. P., S. Levitus, J. I. Antonov, J. R. Reagan, C. Schmid, and R. Locarnini (2012), [Subsurface salinity] Global Oceans [in State of the Climate in 2011], *Bull. Am. Meteorol. Soc.*, *93*(7), S72–S75.

ID: padmavathym Time: 13:48 I Path: //xinchnasjn/01journals/Wiley/3B2/JGRC/Vol00000/140002/APPFile/JW-JGRC140002

Carton, J. A., and E. J. Katz (1990), Estimates of the zonal slope and seasonal transport of the Atlantic North Equatorial Countercurrent, *J. Geophys. Res.*, *95*, 3091–3100, doi:10.1029/JC095iC03p03091.

Dai, A., and K. E. Trenberth (2002), Estimates of freshwater discharge from continents: Latitudinal and seasonal variations, *J. Hydrometeorol.*, *3*, 660–687.

Dessier, A., and J. R. Donguy (1994), The sea surface salinity in the tropical Atlantic between 10°S and 30°N—Seasonal and interannual variations (1977–1989), *Deep Sea Res.*, Part I, *41*, 81–100.

Foltz, G. R., and M. J. McPhaden (2008), Seasonal mixed layer salinity balance of the tropical North Atlantic Ocean, *J. Geophys. Res.*, *113*, C02013, doi:10.1029/2007JC004178.

Foltz, G. R., S. A. Grodsky, J. A. Carton, and M. J. McPhaden (2004), Seasonal salt budget of the northwestern tropical Atlantic Ocean along 38°W, *J. Geophys. Res.*, *109*, C03052, doi:10.1029/2003JC002111.

Garzoli, S. L., A. Ffield, W. E. Johns, and Q. Yao (2004), North Brazil Current retroflection and transports, *J. Geophys. Res.*, *109*, C01013, doi:10.1029/2003JC001775.

Gouretski, V. V., and K. P. Koltermann (2004), WOCE global hydrographic climatology, *Tech. Rep. 35*, Bundesamtes für Seeschiffahrt un Hydrogr.

Grodsky, S. A., N. Reul, G. S. E. Lagerloef, G. Reverdin, J. A. Carton, B. Chapron, Y. Quilfen, V. N. Kudryavtsev, and H.-Y. Kao (2012), Haline hurricane wake in the Amazon/Orinoco plume: AQUARIUS/SACD and SMOS observations, *Geophys. Res. Lett.*, *39*, L20603, doi:10.1029/2012GL053335.

Grodsky, S. A., G. Reverdin, J. A. Carton, and V. J. Coles (2014), Year-to-year salinity changes in the Amazon plume: Contrasting 2011 and 2012 Aquarius/SACD and SMOS satellite data, *Remote Sens. Environ.*, *140*, 14–22, doi:10.1016/j.rse.2013.08.033.

Lagerloef, G., F. Wentz, S. Yueh, H.-Y. Kao, G. C. Johnson, and J. M. Lyman (2012), Aquarius satellite mission provides new, detailed view of sea surface salinity, in *State of the Climate 2011*, *Bull. Am. Meteor. Soc.*, *93*(7), S70–S71.

Large, W. G., and S. G. Yeager (2004), Diurnal to decadal global forcing for ocean and sea-ice models: The datasets and flux climatologies, *NCAR Tech. Note TN-460+STR*, Natl. Cent. for Atmos. Res.

Large, W. G., J. C. McWilliams, and S. C. Doney (1994), Oceanic vertical mixing—A review and a model with a nonlocal boundary layer parameterization, *Rev. Geophys.*, *32*, 363–403.

Liu, H., S. A. Grodsky, and J. A. Carton (2009), Observed subseasonal variability of oceanic barrier and compensated layers, *J. Clim.*, *22*, 6104–6119, doi:10.1175/2009JCLI2974.1.

Lumpkin, R., and Z. Garraffo (2005), Evaluating the decomposition of tropical Atlantic drifter observations, *J. Atmos. Oceanic Technol.*, *22*, 1403–1415.

Lumpkin, R., and S. L. Garzoli (2005), Near-surface circulation in the Tropical Atlantic Ocean, *Deep Sea Res.*, Part I, 52, 495–518, doi:10.1016/j.dsr.2004.09.001.

Maltrud, M., F. Bryan, and S. Peacock (2010), Boundary impulse response functions in a 681 century-long eddying global ocean simulation, *Environ. Fluid Mech.*, *10*, 275–295, 682, doi:10.1007/s10652-009-9154-3.

Mignot, J., C. de Boyer Montégut, A. Lazar, and S. Cravatte (2007), Control of salinity on the mixed layer depth in the world ocean: 2. Tropical areas, *J. Geophys. Res.*, *112*, C10010, doi:10.1029/2006JC003954.

Muller-Karger, F. E., C. R. McClain, and P. L. Richardson (1988), The dispersal of the Amazon's water, *Nature*, *333*, 56–58.

Richardson, P. L., and G. Reverdin (1987), Seasonal cycle of velocity in the Atlantic North Equatorial Countercurrent as measured by surface drifters, current meters, and ship drifts, *J. Geophys. Res.*, *92*, 3691–3708.

Roemmich, D., and the Argo Steering Team (2009), Argo: The challenge of continuing 10 years of progress, *Oceanography*, *22*, 46–55.

Schmitt, R. (2008), Salinity and the global water cycle, *Oceanography*, *21*(1), 12–19.

Xie, S.-P., and J. A. Carton (2004), *Tropical Atlantic variability: Patterns, mechanisms, and impacts, in* Earth's Climate, edited by C. Wang, S. P. Xie, and J. A. Carton, AGU, Washington, D. C., doi:10.1029/147GM07.

Yoo, J.-M., and J. A. Carton (1990), Annual and interannual variation of the freshwater budget in the tropical Atlantic Ocean and the Caribbean Sea, *J. Phys. Oceanogr.*, *20*, 831–845.

AQ1 : Note that Lentz [1995] is not listed in the reference list. Please list or delete the citation.

AQ2 : Please provide publisher location for Gouretski and Koltermann [2004] and Large and Yeager [2004].

USING e-ANNOTATION TOOLS FOR ELECTRONIC PROOF CORRECTION

Required software to e-Annotate PDFs: Adobe Acrobat Professional or Adobe Reader (version 8.0 or above). (Note that this document uses screenshots from Adobe Reader X)
The latest version of Acrobat Reader can be downloaded for free at: http://get.adobe.com/reader/

Once you have Acrobat Reader open on your computer, click on the Comment tab at the right of the toolbar:

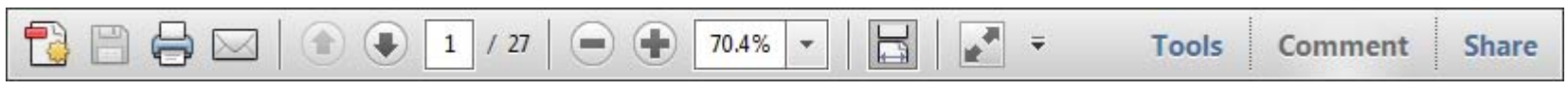

This will open up a panel down the right side of the document. The majority of tools you will use for annotating your proof will be in the Annotations section, pictured opposite. We've picked out some of these tools below:

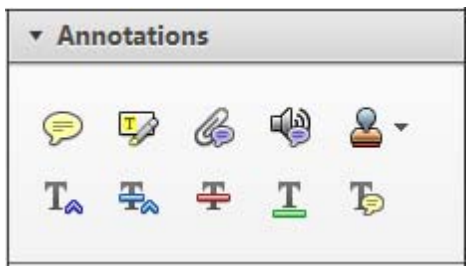

1. Replace (Ins) Tool – for replacing text.

Strikes a line through text and opens up a text box where replacement text can be entered.

How to use it

- Highlight a word or sentence.
- Click on the Replace (Ins) icon in the Annotations section.
- Type the replacement text into the blue box that appears.

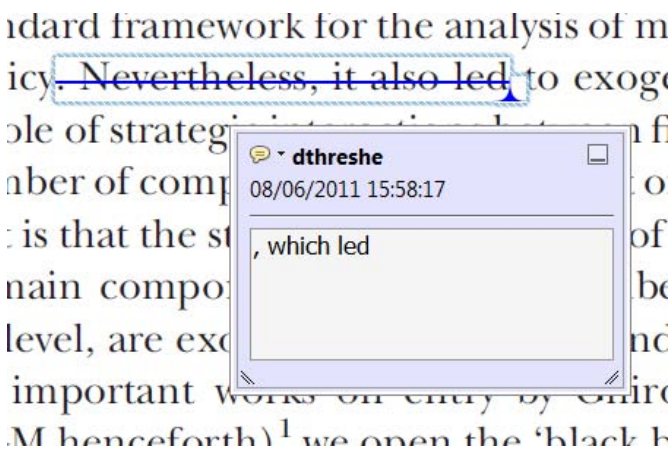

2. Strikethrough (Del) Tool – for deleting text.

Strikes a red line through text that is to be deleted.

How to use it

- Highlight a word or sentence.
- Click on the Strikethrough (Del) icon in the Annotations section.

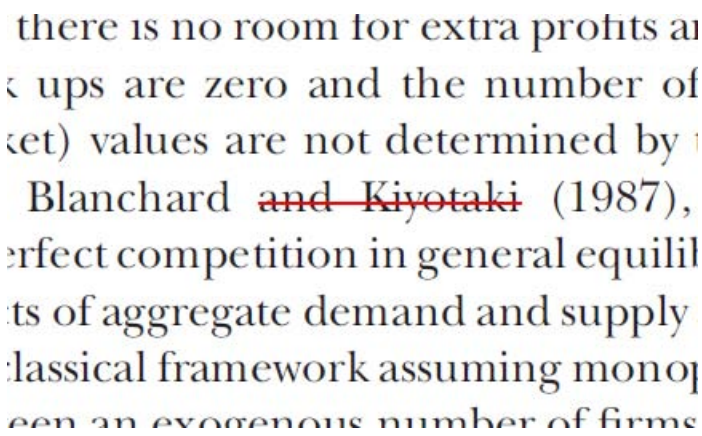

3. Add note to text Tool – for highlighting a section to be changed to bold or italic.

Highlights text in yellow and opens up a text box where comments can be entered.

How to use it

- Highlight the relevant section of text.
- Click on the Add note to text icon in the Annotations section.
- Type instruction on what should be changed regarding the text into the yellow box that appears.

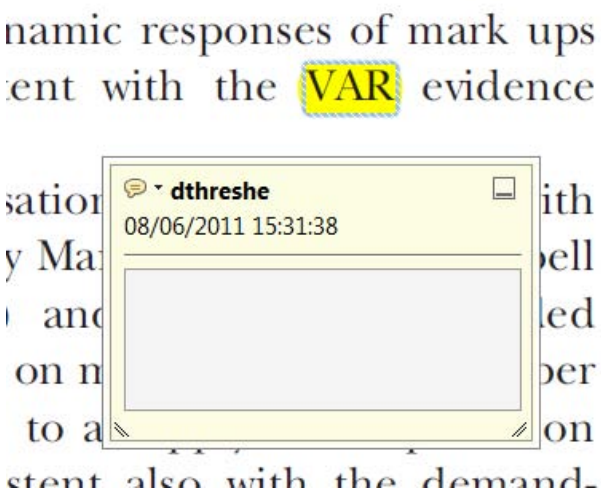

4. Add sticky note Tool – for making notes at specific points in the text.

Marks a point in the proof where a comment needs to be highlighted.

How to use it

- Click on the Add sticky note icon in the Annotations section.
- Click at the point in the proof where the comment should be inserted.
- Type the comment into the yellow box that appears.

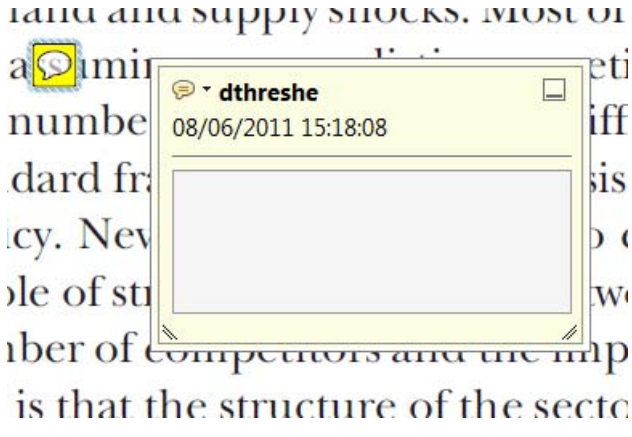

WILEY-BLACKWELL

USING e-ANNOTATION TOOLS FOR ELECTRONIC PROOF CORRECTION

5. Attach File Tool – for inserting large amounts of text or replacement figures.

Inserts an icon linking to the attached file in the appropriate pace in the text.

How to use it

- Click on the Attach File icon in the Annotations section.
- Click on the proof to where you'd like the attached file to be linked.
- Select the file to be attached from your computer or network.
- Select the colour and type of icon that will appear in the proof. Click OK.

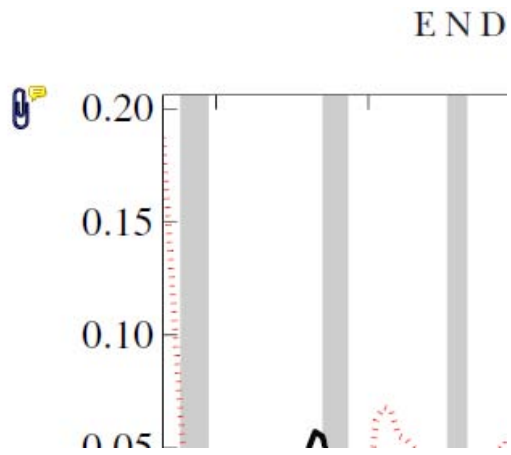

6. Add stamp Tool – for approving a proof if no corrections are required.

Inserts a selected stamp onto an appropriate place in the proof.

How to use it

- Click on the Add stamp icon in the Annotations section.
- Select the stamp you want to use. (The Approved stamp is usually available directly in the menu that appears).
- Click on the proof where you'd like the stamp to appear. (Where a proof is to be approved as it is, this would normally be on the first page).

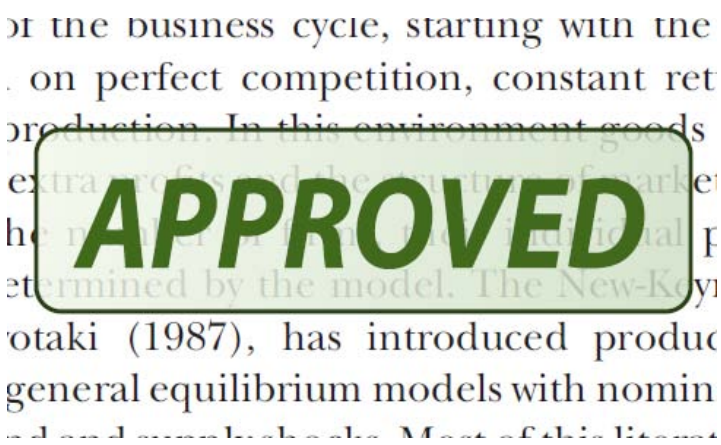

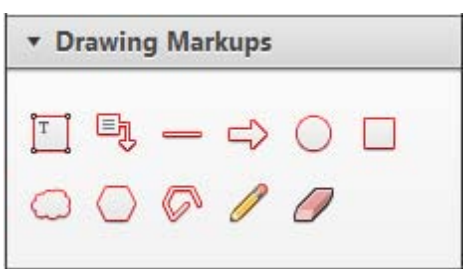

7. Drawing Markups Tools – for drawing shapes, lines and freeform annotations on proofs and commenting on these marks.

Allows shapes, lines and freeform annotations to be drawn on proofs and for comment to be made on these marks..

How to use it

- Click on one of the shapes in the Drawing Markups section.
- Click on the proof at the relevant point and draw the selected shape with the cursor.
- To add a comment to the drawn shape, move the cursor over the shape until an arrowhead appears.
- Double click on the shape and type any text in the red box that appears.

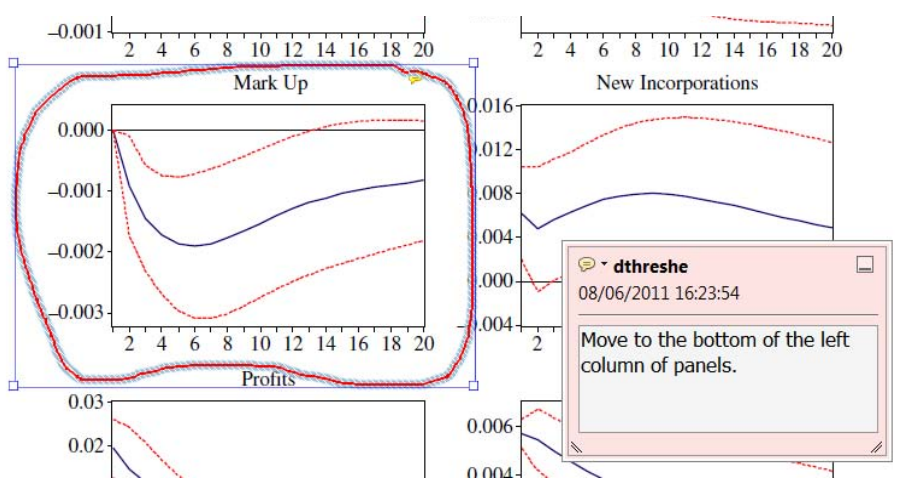

For further information on how to annotate proofs, click on the Help menu to reveal a list of further options: